

# Compensation of thermally induced modal distortions in Faraday isolators.

Efim Khazanov, Nikolay Andreev, Anatoly Mal'shakov, Oleg Palashov, Anatoly Poteomkin,  
Alexander Sergeev, Andrey Shaykin, Victor Zelenogorsky  
*Institute of Applied Physics of Russian Academy of Science, Nizhny Novgorod, Russia*

Igor Ivanov  
*The Research Institute of Materials Science and Technology, Zelenograd, Russia*

Rupal Amin, Guido Mueller, D. B. Tanner, and D. H. Reitze  
*University of Florida*

**Abstract**—Two methods of compensation of thermal lensing in high power terbium gallium garnet (TGG) Faraday isolators have been investigated in detail: compensation by means of an ordinary negative lens and compensation using FK51 Schott glass possessing a negative  $dn/dT$ . Key thermo-optic constants for TGG crystals and FK51 glass were measured. We find that the contribution of the photo-elastic effect to the total thermal lens cannot be neglected either for TGG or for FK51. We define a figure of merit for compensating glass and show that for FK51, an ordinary negative lens with an optimal focus is more efficient, but requires physical repositioning of the lens for different laser powers. In contrast, the use of FK51 as a compensating element is passive and works at any laser power, but is less effective than simple telescopic compensation. The efficiency of adaptive compensation can be considerably enhanced by using a compensating glass with figure of merit more than 50, a crystal with natural birefringence or gel.

**Index Terms**—Laser beam distortion, Laser thermal factors, Optical propagation in anisotropic media, Optical isolators, Thermal variables measurements, Laser accessories, Optical polarization, Faraday effect.

## I. INTRODUCTION

RECENTLY, the average power of solid-state and fiber lasers has overcome the kilowatt barrier and continues to

steadily increase [1, 2]. Therefore, the search for methods of suppressing thermal effects caused by laser absorption in bulk optical elements has become ever more topical. In particular, Faraday isolators (FI) are strongly affected by thermal self-action, since the absorption in magneto-optical media is relatively high. A number of papers have been devoted to investigations of self-induced thermal effects in magneto-optical media [3-16]. The absorption of radiation in optical elements of FIs generates a temperature distribution that is nonuniform over a transverse cross section. This leads to three physical mechanisms affecting the laser radiation: thermal lensing; a nonuniform distribution of the angle of rotation of the polarization plane because of the temperature dependence of the Verdet constant; and the simultaneous appearance of circular birefringence (Faraday effect) and linear birefringence due to the photoelastic effect. The latter two mechanisms alter the polarization state of radiation transmitted through the FI, deteriorating the isolation ratio. This was studied in detail in Ref. [6], where it was shown that the photoelastic effect makes the greatest contribution to the depolarization. In Ref. [5], novel designs of FIs were suggested and theoretically justified, in which the deterioration in the isolation ratio was considerably improved. Further experiments [8, 12] confirmed the high efficiency of the novel designs. The influence of laser beam shape on all these parameters was considered in reference [10]. The dependence of the depolarization ratio in differing FI designs on orientation of magneto-optic crystal was thoroughly investigated in [14]. Another method for compensating depolarization in the FI was suggested and studied in Ref. [15], based on the use of crystalline quartz cut along its optical axis and placed inside a telescope. Taking all of these prior investigations as a whole, the most efficient and convenient design is that of a reciprocal quartz rotator (Fig.1b).

Manuscript received December, 2003. This work was supported in part by National Science Foundation under grants PHY0140110 and PHY0244902. The authors gratefully acknowledge the support of the National Science Foundation.

Efim Khazanov, Nikolay Andreev, Anatoly Mal'shakov, Oleg Palashov, Anatoly Poteomkin, Alexander Sergeev, Andrey Shaykin, Victor Zelenogorsky are with Institute of Applied Physics of Russian Academy of Science, Nizhny Novgorod, Russia (phone: +7-8312-164848; fax: +7-8312-363792; e-mail: khazanov@appl.sci-nnov.ru).

Igor Ivanov is with The Research Institute of Materials Science and Technology, Zelenograd, Moscow region, Russia (e-mail: iia@zelmail.ru).

D.H. Reitze, D.B. Tanner, Rupal Amin, Guido Mueller are with University of Florida, Gainesville, FL 32611-8440, USA (phone: 352-392-3582, fax: 352-392-3591, e-mail: reitze@phys.ufl.edu).

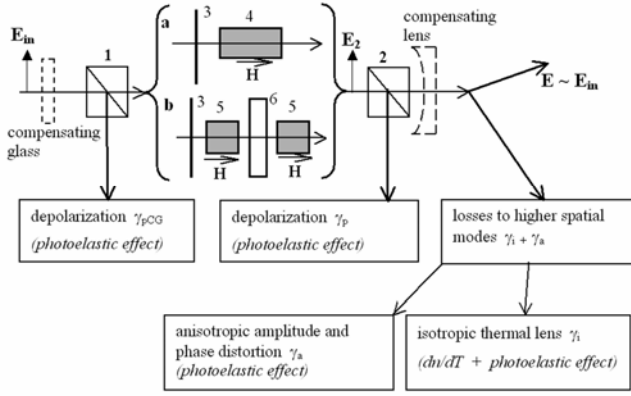


Fig. 1. Overview of power loss mechanisms in the spatial polarization mode after passage of a laser beam through (a) a traditional Faraday isolator (FI) and (b) a birefringence-compensated FI for use at high average powers. Optical components are indicated numerically: 1,2 – polarizers, 3 – half wave plate, 4 – 45 degree Faraday rotator, 5 – 22.5 degree Faraday rotator, 6 – 67.5 degree reciprocal rotator

The isolation ratio is generally the primary but not the only parameter of interest in measuring the performance of an FI. In addition, beam distortions are also induced in these devices through thermal lensing and other mechanisms. In some applications, these characteristics may be as important as the isolation. An example is an FI in a laser interferometer for gravitational wave detection [17] or a Faraday mirror inside a laser oscillator [13, 16, 18] or regenerative amplifier [18].

In the following sections, we consider the performance of two different FI designs – the traditional single element design (Fig. 1a) and the birefringence-compensated design (Fig. 1b) [5]. The latter type employs, instead of a single 45° Faraday rotator, two 22.5° Faraday rotators and a reciprocal polarization rotator placed between them, which rotates the polarization at 67.5°. Let us assume that an incident beam  $\mathbf{E}_{in}$  has horizontal polarization, Gaussian intensity profile with waist  $r_0$  and flat wavefront, i.e., the complex amplitude of the field is given in the form:

$$\mathbf{E}_{in} = \mathbf{x}_0 E_0 \exp(-r^2/2r_0^2) \exp[i(kz - \omega t)] \quad (1)$$

where  $\mathbf{x}_0$  is a unit vector directed along the  $x$  axis,  $r$  is the polar radius,  $k$  is the wave number, and  $\omega$  is the frequency of the laser field. We wish to compare the total power losses in the spatial polarization mode (1) during the first pass (from left to right) of the beam through each isolator design. In both designs, in the absence of thermal effects after the first pass, the beam retains its horizontal polarization and passes through a polarizer 2 (while during the return pass the polarization is altered to vertical and the beam is reflected by a polarizer 1). Because of polarization distortions in the magneto-optical medium, part of the radiation will be reflected by the polarizer 2 after the first pass. The corresponding power loss  $\gamma_p$  (henceforth called *polarization loss*) is determined as a ratio of radiation power reflected from polarizer 2 to radiation power incident on polarizer 2:

$$\gamma_p = \frac{\int_0^{2\pi} d\varphi \int_0^\infty |E_2 \cdot \mathbf{y}_0|^2 r dr}{\int_0^{2\pi} d\varphi \int_0^\infty |E_2|^2 r dr} \quad (2)$$

where  $\mathbf{y}_0$  is a unit vector directed along the  $y$  axis,  $\varphi$  is the azimuthal angle, and  $\mathbf{E}_2$  is the complex amplitude of the field before the polarizer 2. Here (and later), we assume that the clear aperture of FI is such that the aperture losses can be ignored and the integration over  $r$  can be extended to infinity. The component of the field transmitted through the polarizer,  $\mathbf{E}_{2,x}$  is linearly polarized (polarizer 2 is assumed to be ideal), but its transverse structure now differs from the incident Gaussian beam  $\mathbf{E}_{in}$  because of the spatially-dependent amplitude and phase distortions introduced during propagation through the non-uniformly heated magneto-optical medium and the polarizer. We define a second quantity,  $\gamma_s$ , as the difference from unity of projection of the laser field  $\mathbf{E}_{2,x}$  on the ideal Gaussian field (1):

$$\gamma_s = 1 - \frac{\left| \int_0^{2\pi} d\varphi \int_0^\infty E_{2,x} E_{in}^* r dr \right|^2}{\int_0^{2\pi} d\varphi \int_0^\infty |E_{2,x}|^2 r dr \cdot \int_0^{2\pi} d\varphi \int_0^\infty |E_{in}|^2 r dr} \quad (3)$$

Physically, this quantity represents the ‘effective’ power loss from the Gaussian (TEM<sub>00</sub>) beam caused by the introduction of higher order spatial modes transmitted through the polarizer. In the absence of thermal effects,  $\gamma_s = 0$ . Therefore, the total power loss in the TEM<sub>00</sub> spatial polarization mode  $\gamma_t$  during forward propagation through the FI is:

$$1 - \gamma_t = (1 - \gamma_p)(1 - \gamma_s) \quad (4)$$

It has been shown [10, 11] that two different effects contribute to  $\gamma_s$ : an isotropic thermal lens and anisotropic distortions caused by the photoelastic effect. For small distortions ( $\gamma_s \ll 1$ ),  $\gamma_s$  is a sum of two corresponding components: anisotropic amplitude-phase losses  $\gamma_a$  and isotropic phase losses  $\gamma_i$  [10, 11]. Therefore, the total power loss in the spatial polarization mode  $\gamma_t$  during propagation is (for  $\gamma_p \ll 1$ ):

$$\gamma_t = \gamma_p + \gamma_a + \gamma_i \quad (5)$$

The first two components are related to depolarization caused by the photoelastic effect, whereas the latter component represents pure optical path (phase) distortions induced by isotropic thermal lens. These losses are indicated schematically on Fig. 1. Note that a contribution to the isotropic thermal lens is made by both the temperature dependence of refractive index and the “isotropic” part of the photoelastic effect (see below). It has been shown previously [10, 11] that  $\gamma_i$  is the same for all FI designs.

The temperature distribution in the optical element and, consequently, the distribution of phase of an aberrated laser

beam are close to parabolic. Therefore, the majority of the phase distortions can be compensated by means of an ordinary lens or a telescope (shown as a dashed line in Fig. 1), which introduces additional curvature in the wavefront. Throughout the text, we shall henceforth call this method of compensation "telescopic compensation", indicating corresponding losses by subscript "TC". Obviously, the isotropic thermal lens is not totally compensated, since the ordinary lens can compensate only for parabolic phase, but the thermal lens has a more complex profile. For small distortions, it has been shown that the isotropic losses introduced by the thermal lens can be reduced approximately by a factor of 15, provided the position and focus of the compensating lens is chosen optimally [10, 11]:

$$\gamma_{iTC} \approx \gamma_{iNC} / 15$$

Here and further the subscript "NC" indicates that there is no compensation present and the subscript  $i$  refers to the isotropic component of depolarization.

Alternatively, an adaptive method for compensating the thermal lens was suggested and experimentally studied [19, 20]. Essentially, it consists of a compensating glass (CG) placed before (or after) polarizer 1 (e.g., Schott glass FK51; indicated as the dashed line in Fig. 1). The parameters of the CG are chosen such that the thermal lens has the same amplitude and shape as in FI but, at the same time, is negative (in many magneto-optic materials it is positive). If we do not take into account propagation of the beam between CG and FI, the isotropic losses are totally compensated:

$$\gamma_{iAC} = 0$$

Here and later the subscript "AC" denotes the adaptive compensation. It has been shown that the influence of propagation can be insignificant for reasonable adaptive compensation geometries [19].

The adaptive method has two advantages over the telescopic compensation: there is no need in adjustment when laser power is changed, and the accuracy of isotropic compensation is higher. However, a disadvantage of the adaptive method is that the photoelastic effect in the CG leads to additional distortions and, consequently, to losses in the spatial polarization mode. By analogy with losses introduced into FI, these losses can be subdivided into polarization losses  $\gamma_{pCG}$ , (power reflected by polarizer 1), and anisotropic amplitude-phase losses  $\gamma_{aCG}$  (see Fig. 1).

As we show in this paper, the above two compensation methods can compensate only for  $\gamma_i$ . The telescopic method is less efficient but does not lead to additional losses  $\gamma_p$  and  $\gamma_a$ . The adaptive method totally compensates for  $\gamma_i$  (if we ignore propagation), but increases losses  $\gamma_p$  and  $\gamma_a$  because of the photoelastic effect in the CG. This effect was not considered by Mueller et. al. [19]. In section 2 of this paper, we present a detailed comparison of the two compensation methods – telescopic and adaptive – considering all thermal effects both in the magneto-optic crystal and in compensating glass. Based on these results, we determine physical constants and define a figure-of-merit for the compensating glass that predicts the

efficiency of the adaptive method. In section 3, we report on the results of measurement of key thermo-optical constants for TGG crystal and FK51 glass. We also describe experimental results of compensation of the thermal lens in FI with a quartz rotator (Fig. 1b) using FK51 glass. In section 4, our results will be discussed and our conclusions are summarized in section 5.

## II. THE EFFICIENCY OF MODE DISTORTION COMPENSATION.

The calculation of total losses without compensation  $\gamma_{iNC}$  and with telescopic compensation  $\gamma_{iTC}$  have been previously [10, 11] derived analytically. Here we shall calculate, by analogy with those papers, the total loss in case of adaptive compensation  $\gamma_{iAC}$  and shall compare the results with  $\gamma_{iNC}$  and  $\gamma_{iTC}$ . We assume that the Rayleigh range of the beam is much greater than the length of FI, even taking into account induced distortions, i.e., diffractive propagation effects can be totally neglected. It is seen from expressions (2-4) that for determining the total loss  $\gamma_{iAC}$ , it is enough to find the field before a second polarizer  $E_2$ . This value can be found by applying the formalism of the Jones polarization matrices:

$$E_2 = F(\delta_c = \pi/2, \delta_l, L) L_2(3\pi/8) P_x G(\delta_{CG}) E_{in} \quad (6a)$$

$$E_2 = F(\delta_c = \pi/4, \delta_l/2, L/2) R(-3\pi/8) \left| \begin{array}{l} F(\delta_c = \pi/4, \delta_l/2, L/2) \\ L_2(\pi/16) P_x G(\delta_{CG}) E_{in} \end{array} \right. \quad (6b)$$

Here and later letters "a" and "b" correspond to formulas for FI in Fig. 1a and b.  $F$ ,  $L_2$ ,  $R$ ,  $P_x$ , and  $G$  denote the Jones matrices for the Faraday rotator,  $\lambda/2$  waveplate, quartz rotator, polarizer, and compensating glass respectively,  $\delta_l$  is the phase difference between linear eigenpolarizations along the entire length of the magneto-optical medium  $L$ ; and  $\delta_c$  is the phase difference between circular eigenpolarizations. The matrices for the rotator,  $\lambda/2$  plate and polarizer are well known:

$$R(\beta_R) = \begin{pmatrix} \cos \beta_R & \sin \beta_R \\ -\sin \beta_R & \cos \beta_R \end{pmatrix} \quad L_2(\beta_L) = \begin{pmatrix} \cos 2\beta_L & \sin 2\beta_L \\ \sin 2\beta_L & -\cos 2\beta_L \end{pmatrix} \quad P_x = \begin{pmatrix} 1 & 0 \\ 0 & 0 \end{pmatrix} \quad (7)$$

where  $\beta_{R,L}$  are the rotation angles. Bearing in mind the linear birefringence, a Faraday rotator that rotates the polarization plane by an angle  $\delta_c/2$  can be described by the following Jones matrix [21, 22]

$$F(\delta_c, \delta_l, L, \Psi) = \exp(ikLn) \cdot \sin \frac{\delta}{2} \cdot \begin{pmatrix} \cot \frac{\delta}{2} - i \frac{\delta_l}{\delta} \cos 2\Psi & -\frac{\delta_c}{\delta} - i \frac{\delta_l}{\delta} \sin 2\Psi \\ \frac{\delta_c}{\delta} - i \frac{\delta_l}{\delta} \sin 2\Psi & \cot \frac{\delta}{2} + i \frac{\delta_l}{\delta} \cos 2\Psi \end{pmatrix} \quad (8)$$

where

$$\delta^2 = \delta_l^2 + \delta_c^2 \quad (9)$$

$\Psi$  is the angle of inclination of the linear eigenpolarization

relative to the  $x$ -axis (see Fig. 2),  $n$  is the refractive index averaged for two eigenpolarizations. We shall consider here only cylindrical optical elements and only two most common orientations – [001] (with an angle  $\theta$  between the crystallographic axis and the  $x$  axis) and [111]. Note that for the traditional FI design (Fig. 1a), the best orientation is [001], whereas [111] is the optimal crystal orientation for the birefringence compensated design (Fig. 1b) [14].

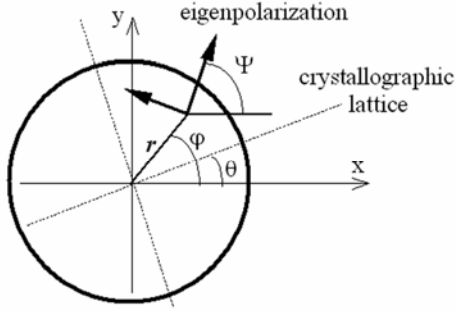


Fig. 1. Crystal cross-section showing the crystallographic axes and eigenpolarizations for the calculations described in the text.

The value of  $n(r)$  is determined by the temperature distribution  $T(r)$ . The expression for  $n(r)$  can be found, e.g., in [23]:

$$n(r) = n(0) + [T(r) - T(0)]P \quad (10)$$

where  $P$  for the crystal orientations under consideration is:

$$P_{[001]} = \frac{dn}{dT} - \left( \frac{1}{L} \frac{dL}{dT} \right) \frac{n_0^3}{4} \frac{1+\nu}{1-\nu} \cdot (p_{11} + p_{12}) \quad (11)$$

$$P_{[111]} = P_{[001]} - Q \frac{\xi - 1}{3}$$

$$Q = \left( \frac{1}{L} \frac{dL}{dT} \right) \frac{n_0^3}{4} \frac{1+\nu}{1-\nu} \cdot (p_{11} - p_{12}) \quad (12)$$

$$\xi = \frac{2p_{44}}{p_{11} - p_{12}} \quad (13)$$

and  $n_0$ ,  $\nu$ ,  $(1/L)(dL/dT)$ ,  $p_{ij}$  are the non-excited ("cold") refractive index, Poisson's ratio, thermal expansion coefficient, and photoelastic coefficients of the magneto-optic medium, respectively.

The exponential phase factor in expression (8) does not affect the polarization distortions and represents an isotropic thermal lens. The temperature dependence of the refractive index and the "isotropic" part of the photoelastic effect contribute to this lens (see two corresponding components in expression (11) for  $P_{[001]}$ ). In papers [24, 25], it was shown that the contribution of the thermal expansion along  $z$ -direction of the medium to the thermal lens is negligibly small, as compared to the temperature dependence of the refractive index. Therefore, we assume that length  $L$  is independent of temperature.

The values of  $\delta_l$  and  $\Psi$  are determined by the photoelastic effect and depend on the temperature gradient  $dT(r)/dr$  [23, 26]:

$$\left\{ \begin{array}{l} \delta_l(r, \varphi) = \frac{4\pi L}{\lambda} Q \left[ \frac{1 + \xi^2 \tan^2(2\varphi - 2\theta)}{1 + \tan^2(2\varphi - 2\theta)} \right]^{1/2} \frac{1}{r^2} \int_0^r r^2 \frac{dT}{dr} dr \\ \tan(2\Psi - 2\theta) = \xi \tan(2\varphi - 2\theta) \quad \text{for [001]} \end{array} \right. \quad (14)$$

$$\left\{ \begin{array}{l} \delta_l(r, \varphi) = \frac{4\pi L}{\lambda} Q \left[ \frac{1 + 2\xi}{3} \right] \frac{1}{r^2} \int_0^r r^2 \frac{dT}{dr} dr \\ \Psi = \varphi \quad \text{for [111]} \end{array} \right. \quad (15)$$

where  $\lambda$  is a wavelength. As seen, the expressions for  $\delta_l$  and  $\Psi$  for the [001] orientation transform into expressions for  $\delta_l$  and  $\Psi$  for the [111] orientation, when  $\xi$  is substituted by unity and  $Q$  – by  $Q(1+2\xi)/3$ . Therefore, we shall henceforth only give expressions only for the [001] orientation, bearing in mind that corresponding formulas for the [111] orientation can be obtained by these substitutions. We also drop the [111], [001] subscripts from  $P, Q$  when referring to TGG.

The temperature distribution  $T(r)$  can be easily found from the thermal conductivity equation for infinitely long cylinder

$$T(r) - T(0) = -\frac{\alpha P_0}{2\pi\kappa} \int_0^r \frac{1 - \exp(-r^2/r_0^2)}{r} dr \quad (16)$$

where  $\alpha$  and  $\kappa$  are the absorption coefficient and the thermal conductivity of the magneto-optical medium, and  $P_0$  is the laser radiation power.

Thus, expressions (9-16) fully determine the matrix of the Faraday rotator (8). From a physical point of view, the compensating glass is equivalent to a Faraday element without a magnetic field present. Consequently, its matrix  $\mathbf{G}$  is simply matrix  $\mathbf{F}$  at  $\delta_c = 0$ . All constants of the magneto-optical medium ( $L, n_0, \nu, p_{ij}, \alpha, \kappa, P, Q$ ) must be replaced with appropriate constants of compensating glass ( $L_{CG}, n_{0CG}, \nu_{CG}, p_{ijCG}, \alpha_{CG}, \kappa_{CG}, P_{CG}, Q_{CG}$ ). Note that  $\xi_{CG}$  for any glass is equal to unity. Therefore, substitution of matrices  $\mathbf{F}$  and  $\mathbf{G}$ , and expression (7) into expression (6), and then substitution of the result into expressions (2-4), yield:

$$\gamma_{iAC} = \gamma_{pAC} + \gamma_{aAC} + \gamma_{iAC} \quad (17)$$

$$\left\{ \begin{array}{l} \gamma_{pAC} = \frac{A_1}{\pi^2} \cdot p^2 \xi^2 + \frac{A_1}{8} \cdot p_{CG}^2 \\ \gamma_{aAC} = \frac{A_1}{\pi^2} p^2 + \frac{A_1}{8} p_{CG}^2 + \frac{A_1 \xi}{\pi \sqrt{8}} p \cdot p_{CG} \\ \gamma_{iAC} = \frac{A_3}{4} (p_i + p_{iCG})^2 \end{array} \right. \quad (18a)$$

$$\left\{ \begin{array}{l} \gamma_{pAC} = \frac{A_1}{\pi^2} (2 - \sqrt{2}) p^2 + \frac{A_1}{8} p_{CG}^2 \\ \gamma_{aAC} = \frac{A_1 (2 - \sqrt{2})}{\pi^2} \xi^2 p^2 + \frac{A_1}{8} p_{CG}^2 + \frac{A_1 (\sqrt{2} + \xi - 1)}{\pi \sqrt{8}} p p_{CG} \end{array} \right. \quad (18b)$$

$$\gamma_{iAC} = \frac{A_3}{4} (p_i + p_{iCG})^2$$

where we have defined the following quantities and constants:

$$A_1 = \int_0^\infty \left( \frac{1}{y} - \frac{\exp(-y)}{y} - 1 \right) \frac{dy}{\exp(y)} \cong 0.137 \quad (19)$$

$$A_3 = \int_0^\infty f^2(y) \exp(-y) dy - \left[ \int_0^\infty f(y) \exp(-y) dy \right]^2 \cong 0.268$$

$$f(y) = \int_0^y \frac{1 - \exp(-y')}{y'} dy' \quad (20)$$

$$p_i = \frac{L}{\lambda} \frac{\alpha P}{\kappa} P_0 \quad p = \frac{L}{\lambda} \frac{\alpha Q}{\kappa} P_0 \quad (21)$$

$$p_{iCG} = \frac{L_{CG}}{\lambda} \frac{\alpha_{CG} P_{CG}}{\kappa_{CG}} P_0 \quad p_{CG} = \frac{L_{CG}}{\lambda} \frac{\alpha_{CG} Q_{CG}}{\kappa_{CG}} P_0$$

Analytic expressions (17,18) are obtained for the case of weak distortions, i.e., they are valid at  $\gamma \ll 1$ . In our calculations, we assumed that the angle  $\theta$  has its optimum value [10, 11]

$$\theta_{opt} = -\pi/8 \quad (22a)$$

$$\theta_{opt} = 5\pi/16 \quad (22b)$$

It is clear from expression (18) that for compensation of the isotropic part of losses  $\gamma_i$  the following condition must be obeyed

$$p_{iCG} = -p_i \quad (23)$$

from which, taking into account (21), we obtain

$$p_{CG} = -\frac{P}{Q} \frac{Q_{CG}}{P_{CG}} p \quad (24)$$

Thus, the key parameter of the compensating glass is the ratio  $P_{CG}/Q_{CG}$ , and the higher this ratio, the better the glass. Specifically, if this ratio is much more than that for the magneto-optical crystal, then losses associated with anisotropy thermally induced in the glass can be ignored.

For comparison, we give expressions from Refs. [10, 11] for the total loss without compensation

$$\gamma_{iNC} = \gamma_{pNC} + \gamma_{aNC} + \gamma_{iNC} \quad (25)$$

$$\left\{ \begin{array}{l} \gamma_{pNC} = p^2 \frac{A_1}{\pi^2} \xi^2 \quad \gamma_{aNC} = p^2 \frac{A_1}{\pi^2} \\ \gamma_{iNC} = \frac{A_3}{4} p_i^2 \end{array} \right. \quad (26a)$$

$$\left\{ \begin{array}{l} \gamma_{pNC} = \frac{p^2 A_1}{\pi^2} (2 - \sqrt{2}) \\ \gamma_{aNC} = \frac{p^2 A_1}{\pi^2} (2 - \sqrt{2}) \xi^2 \quad \gamma_{iNC} = \frac{A_3}{4} p_i^2 \end{array} \right. \quad (26b)$$

In the case of telescopic compensation, the first two components remain unchanged, whereas the third one is reduced approximately by a factor of 15 [10, 11]:

$$\gamma_{iTC} = \gamma_{pNC} + \gamma_{aNC} + \frac{A_4}{A_3} \gamma_{iNC} \quad (27)$$

$$A_4 = \frac{\left[ \int_0^\infty (f(y) - 0.5y)^2 \exp(-y) dy \right]}{\left[ \int_0^\infty (f(y) - 0.5y) \cdot \exp(-y) dy \right]^2} \cong 0.0177 \cong 0.0660 A_3 \quad (28)$$

(Note that in equ. (27) for telescopic compensation ('TC'), we assume that the absorption in compensating lens is essentially zero, leading to negligible contributions for  $\gamma_{iAC}$  and  $\gamma_{pAC}$ .) The comparison of (17) and (27) yields a condition, at which  $\gamma_{iAC} < \gamma_{iTC}$ , i.e., compensation with glass is more efficient than with a lens or a telescope:

$$\left| \frac{P_{CG}}{Q_{CG}} \right| > \sqrt{\frac{A_1}{A_4} \left( \sqrt{1 + \frac{A_1}{2A_4} \left[ \frac{\xi Q}{\pi P} \right]^2} + \sqrt{\frac{A_1}{A_4} \frac{\xi}{\pi \sqrt{2}} \left| \frac{Q}{P} \right|} \right)} \quad (29a)$$

$$\left| \frac{P_{CG}}{Q_{CG}} \right| > \sqrt{\frac{A_1}{A_4} \left( \sqrt{1 + \frac{A_1}{2A_4} \left[ \frac{(\sqrt{2} + \xi - 1) Q}{\pi P} \right]^2} + \sqrt{\frac{A_1}{A_4} \frac{(\sqrt{2} + \xi - 1)}{\pi \sqrt{2}} \left| \frac{Q}{P} \right|} \right)} \quad (29b)$$

Here we took into account that  $Q < 0$ ,  $Q_{CG} < 0$ ,  $P_{CG} < 0$ ,  $P > 0$  (see below). The ratio  $P/Q$  has not been measured for the TGG crystal, which is most commonly used in FI; nor has it been found for the FK51 glass. Note that for laser Nd glasses, this ratio varies within a wide range: from 0.5 to 500 [27]. Therefore, the measurement of parameters  $P$  and  $Q$  for TGG and FK51 becomes important, and additional experiments are required to confirm the efficiency of the adaptive method for compensating the thermal lens.

### III. MEASUREMENT OF THERMOOPTICAL CONSTANTS OF TGG CRYSTAL AND FK51 GLASS.

From expressions (17, 23-25, 27), energy losses in the spatial polarization mode  $\gamma_t$  (both with and without compensation of the thermal lens) are totally determined by parameters  $p$ ,  $p_i$ ,  $\xi$ ,  $Q_{CG}/P_{CG}$ , and the lower these parameters, the lower  $\gamma_t$ . Therefore, we must determine the following constants:  $\kappa$ ,  $\alpha$ ,  $Q$ ,  $P$  and  $\xi$  for a magneto-optic medium (here we consider TGG only) and  $Q_{CG}$ ,  $P_{CG}$  for compensating glass (FK51). The thermal conductivity of TGG is  $\kappa = 7.4$  W/Km. The absorption coefficient of TGG  $\alpha$  can vary significantly (up to a factor of four) from sample to sample [14, 19, 28], and the value of  $\xi$  for TGG has been recently measured in Refs. [14, 28]:  $\xi = 2.25 \pm 0.2$ . More difficult is to measure the thermo-optical constants  $Q$  and  $P$  (as well as  $Q_{CG}$ ,  $P_{CG}$ ), because of the difficulty in measuring their constituent constants, in particular, photoelastic coefficients

$p_{ij}$ . In subsection 3.1, we shall describe measurements of  $Q$ , carried out using a technique reported in Ref. [6]. In subsection 3.2, a scanning Hartmann sensor will be described, which we utilized for measuring  $P$ . The results of the measurements will be summarized in subsection 3.3.

#### A. Measurement of thermo-optical constant $Q$ .

All known direct measurements of  $Q$  to date have been made by means of an interferometric setup [29, 30]. The root-mean-square error of these measurements is typically 5–15% [23]. Here, we employ a simple measurement technique [6] which provides the same accuracy. It consists of measuring the depolarization of high-power laser radiation propagating in an absorbing medium in the absence of a magnetic field  $\gamma_{H=0}$  as a function of laser radiation power:

$$\gamma_{H=0} = p^2 \frac{A_1}{8} (1 + (\xi - 1)^2 \cos^2(2\theta)) \quad (30)$$

If all values, except  $Q$  in the right-hand side of equ. (30), are known, then by measuring  $\gamma_{H=0}$ , one can determine the constant  $Q$ , using it as a fitting parameter. We performed such measurements for FK51 Schott glass and for a [001] TGG crystal produced at the Research Institute of Materials Science and Technology, Zelenograd, Russia (RIMST). The measurement results are shown in Fig. 3. At small  $p$ , the depolarization  $\gamma_{H=0}$  does not depend on power, since it is determined by "cold" birefringence. At higher powers, the coincidence between experimental values and formulas (30) is fairly good.

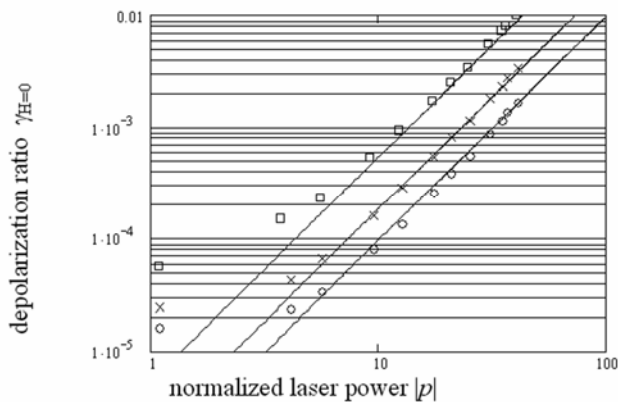


Fig. 3. Measurement of zero-field depolarization  $\gamma_{H=0}$  as a function of  $p$  (see equ. 21 for definition of  $p$ ) for a 48mm long TGG crystal (manufactured by RIMST) at  $\theta=0$  (squares) and  $\theta=\pi/4$  (circles) as well as for FK51 glass 67mm length (crosses). Theoretical curves are plotted according (30) at  $\alpha_{TGG}Q_{TGG}=1.2 \cdot 10^{-8} \text{K}^{-1} \text{cm}^{-1}$ ,  $\alpha_{FK51}Q_{FK51}=0.15 \cdot 10^{-8} \text{K}^{-1} \text{cm}^{-1}$ .

The transmission and residual reflection of anti-reflective coating were measured for this particular TGG crystal (length 48 mm, diameter 9 mm). Based on these data, we calculated the absorption. The transmission was measured at a wavelength of 1053 nm both for one and two passes of the radiation through the crystal. In the both cases, the value of the absorption was the same,  $\alpha_{TGG}=(4.8 \pm 0.4) \times 10^{-3} \text{cm}^{-1}$ . Knowing  $\alpha_{TGG}$  from Fig. 3 we obtain the following value

$$Q_{TGG} = -(2.6 \pm 0.4) \times 10^{-6} \text{K}^{-1} \quad (31)$$

The sign of  $Q$  for TGG and FK51 (see below) was determined by the technique reported in [31]. The absorption of FK51 glass in catalogue is  $\alpha_{FK51}=2.4 \cdot 10^{-3} \text{cm}^{-1}$ . Using  $\alpha_{FK51}=2.4 \cdot 10^{-3} \text{cm}^{-1}$  from Fig. 3 we obtain

$$Q_{FK51} = -0.63 \times 10^{-6} \text{K}^{-1} \quad (32)$$

The measured value of  $Q_{FK51}$  (32) is close to that in catalogue  $Q_{FK51} = -(0.53-0.59) \cdot 10^{-6} \text{K}^{-1}$  for a wavelength of 589 nm. For some glasses, it is known that  $Q$  very weakly depends on a wavelength [9]. However, keeping in mind that the accuracy of  $\alpha_{FK51}=2.4 \cdot 10^{-3} \text{cm}^{-1}$  may be not very high, it is important to note that the value of the product  $\alpha_{FK51}Q_{FK51}$  is measured with high accuracy:

$$\alpha_{FK51}Q_{FK51} = -(0.15 \pm 0.02) \times 10^{-8} \text{K}^{-1} \text{cm}^{-1} \quad (33)$$

#### B. Use of a scanning Hartmann sensor for thermal lens measurements.

The detailed description of the operation of the scanning Hartmann sensor can be found elsewhere [28]. Here, we briefly describe its operation in measurements of thermal lensing. An optical schematic of the experiment is illustrated in Fig. 4.

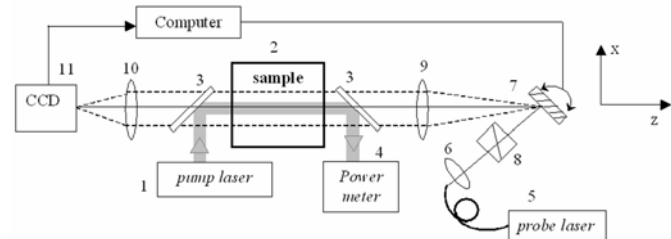


Fig. 3. Experimental schematic diagram for the scanning Hartmann sensor described in the text. Optical components are indicated numerically: 1 – pump laser, 2 – sample, 3 – mirror, 4 – power meter, 5 – probe laser, 6 – collimating lens, 7 – rotating mirror, 8 – polarizer, 9, 10 – lens, 11 – CCD-camera.

The laser beam from a 40 W 1053 nm, CW Nd:YLF single-transverse mode laser (indicated as '1' in the figure) is used to heat the optic under test (2). Dichroic mirrors (3) are used to couple the beam into and out of the sample, with the laser power monitored using a power meter (4). An 850 nm, CW single-mode diode 'probe' laser (5) with fiber output for mode cleaning is collimated by a lens (6), with the output polarization set by a polarizer (8). This scheme provides a constant spatial structure of the probe beam. A rotating mirror 7, placed on the axis of a computer-controlled galvanometric scanner, changes the angular pointing of the beam. The solid line in Fig. 3 indicates the beam path in the midposition of the mirror (7), and the dotted lines – in two end positions. The rotational axis of the mirror (7) is located at the focal plane of a lens (9) with focal length 295 mm such that angular scanning of the mirror (7) resulted in a parallel movement of the beam along diameter of the sample. In the presence of a thermal lens, the probe beam transmitted through the sample deviates from its initial direction by a small but measurable angle. This angle leads to a corresponding shift of the beam in the focal plane of a second

$f = 600\text{mm}$  lens (10), which focuses the probe beam onto a CCD camera (11) located a distance  $f$  from the lens. The signal from the CCD camera is sent to a computer, which determines and compares the coordinates of the beam's centroid position before and after heating the sample. By scanning the galvanometer, we are able to measure the differential optical path difference as a function of the heating power with a resolution of  $\lambda/500$ .

In contrast to the traditional Hartmann sensor [20, 32], in which the entire aperture of the sample is measured simultaneously at many points, in this method one has to scan the beam over the sample aperture point by point. Although this procedure is time-consuming, it avoids problems associated with overlapping of different beams which are frequently encountered in the traditional Hartmann sensor.

### C. Measurement of thermo-optical constant $P$ .

To eliminate depolarization of radiation from a probe laser in the sample, we used only  $r$ - (the field along the polar radius) and  $\varphi$ - (the field along the polar angle) polarizations. Measurements were made in the absence of a magnetic field for four cases: TGG with the [111] orientation; TGG with the [001] orientation at  $\theta=0$ ; TGG with the [001] orientation at  $\theta=\pi/4$ ; and FK51 glass. By analogy with section 2, it can be easily shown that in the first three cases the phase  $\Delta(u)$  for  $r$ - and  $\varphi$ -polarizations of the probe beam after a pass through a sample with the length  $L_s$  is described by the following expressions:

$$\left\{ \begin{array}{l} \Delta_{r,\varphi}^{[111]}(u) = -\frac{L_s}{2\lambda} \frac{\alpha P_0}{\kappa} \left( P_{[111]} \left[ \int_0^u \frac{1-\exp(-t)}{t} dt \right] \mp \right. \\ \left. \mp Q \frac{1+2\xi}{3} \cdot \frac{u+\exp(-u)-1}{u} \right) \\ \Delta_{r,\varphi}^{[001]}(u, \theta=0) = -\frac{L_s}{2\lambda} \frac{\alpha P_0}{\kappa} \left( P_{[001]} \left[ \int_0^u \frac{1-\exp(-t)}{t} dt \right] \mp \right. \\ \left. \mp Q \xi \frac{u+\exp(-u)-1}{u} \right) \\ \Delta_{r,\varphi}^{[001]} \left( u, \theta = \frac{\pi}{4} \right) = -\frac{L_s}{2\lambda} \frac{\alpha P_0}{\kappa} \left( P_{[001]} \left[ \int_0^u \frac{1-\exp(-t)}{t} dt \right] \mp \right. \\ \left. \mp Q \frac{u+\exp(-u)-1}{u} \right) \end{array} \right. \quad (34)$$

Here  $u=x^2/r_0^2$  is the scaled transverse coordinate. We use  $x$  to denote the radial distance from the center of the crystal to reflect that our experiments scan the distortion in one dimension, see Fig. 3. For the glass, we can use any of the three expressions at  $\xi=1$ . Note that the distribution of the isotropic term (the first component) of the thermal lens is the same as the temperature distribution (16), whereas the anisotropic (the second component) part has a different shape.

With the measurements of  $\alpha$  and  $Q$ , all values except  $P$  in equation (34) are known.  $P$  was used as a fitting parameter. Measurements for FK51 Schott glass, two TGG crystals with the [001] orientation (from Electro-optic technologies (EOT) and RIMST) and one TGG crystal with [111] orientation (from Litton) were carried out. The dependences  $\Delta(r)$  for glass and the RIMST crystal are presented in Fig. 5. The figure clearly shows good coincidence between theoretical (34) and experimental curves, demonstrating that the measurement accuracy of  $P$  was high and the sign of  $Q$  was properly determined.

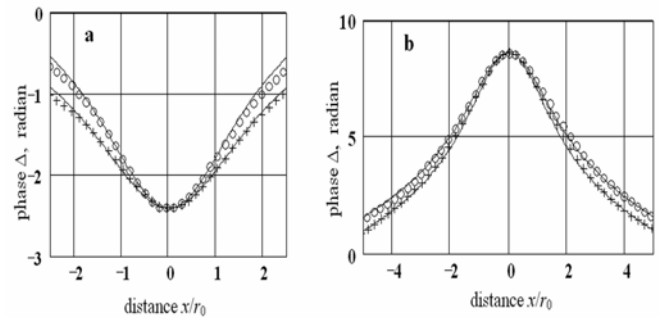


Fig. 5. Probe laser optical path difference after propagating through (a) a 48mm long TGG crystal at  $\theta=\pi/4$  and (b) FK51 glass 67mm length when heated by 38W pump laser. Circles –  $\varphi$ -polarization, crosses –  $r$ -polarization. Theoretical curves are plotted according to equ. (34) at  $\alpha_{TGG} P_{TGG} = 1.5 \cdot 10^{-8} \text{ K}^{-1} \text{ cm}^{-1}$ ,  $\alpha_{FK51} P_{FK51} = -0.41 \cdot 10^{-8} \text{ K}^{-1} \text{ cm}^{-1}$

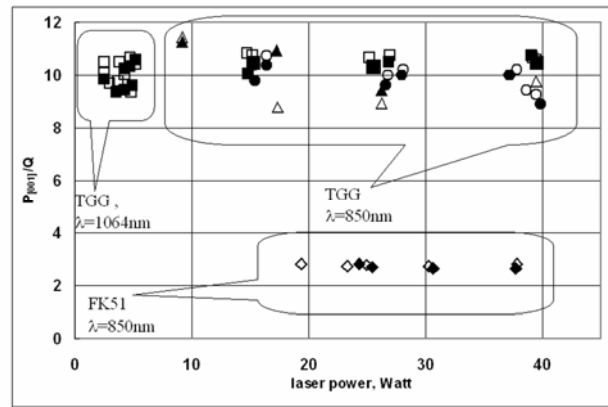


Fig. 6. The ratio  $P_{[001]}/Q$  for FK51 glass (diamonds) and TGG crystals grown by EOT (circles), Litton (triangles), and RIMST (squares). Filled symbols correspond to  $\varphi$ -polarization, open symbols –  $r$ -polarization.

The measurements demonstrated the absence (within the experimental error) of the dependence of  $P$  on power of the heating laser, and the absence of the dependence of  $P_{[001]}/Q$  on a particular TGG sample (see Fig. 6). Knowing the absorption of the RIMST crystal  $\alpha_{TGG} = (4.8 \pm 0.4) \cdot 10^{-3} \text{ cm}^{-1}$ , from Fig. 5a we obtain the value of  $P_{[001]}$

$$P_{[001]} = (26 \pm 4) \cdot 10^{-6} \text{ K}^{-1} \quad (35)$$

Using  $\alpha_{FK51} = 2.4 \cdot 10^{-3} \text{ cm}^{-1}$ , from Fig. 5b for the FK51 glass we obtain

$$P_{FK51} = -1.7 \cdot 10^{-6} \text{ K}^{-1} \quad (36)$$

Again, although the accuracy of the value  $\alpha_{FK51} = 2.4 \cdot 10^{-3} \text{ cm}^{-1}$  may be not high (see above), it is important to note that

the value of the product  $\alpha_{FK51}P_{FK51}$  is measured with high accuracy:

$$\alpha_{FK51}P_{FK51} = -(0.41 \pm 0.06)10^{-8} \text{ K}^{-1}\text{cm}^{-1} \quad (37)$$

which, considering (33), yields the critical parameter  $P/Q$  (see section 2):

$$P_{FK51}/Q_{FK51} = 2.8 \pm 0.4 \quad (38)$$

The accuracy of the measurement does not depend on the uncertainty concerning the value of  $\alpha_{FK51}$ . It is seen from Fig. 5 that the astigmatism of the thermal lens is considerably higher for FK51 than for TGG, which is a result of lower ratio  $P/Q$ .

It is worth noting that the measurements of  $P$  are made at a wavelength of 815 nm. To verify that  $P$  weakly depends on wavelength, we performed measurements at a wavelength of the probe laser of 1060 nm. Since the wavelength of the probe and heating lasers are very close, we used a more sophisticated experimental technique described in Ref. [28]. A sample was heated not by a Gaussian but rather a  $\Pi$ -shaped (flat-top) beam with a diameter equal to the crystal diameter. Corresponding points are shown in Fig. 6. It is evident that the value of  $P_{[001]}$  for TGG is the same, within the experimental error, for these wavelengths.

#### D. Experimental determination of thermal lens compensation in FI using FK51 glass

Our scanning Hartmann sensor was also used to experimentally verify the adaptive compensation method [19] on a birefringence-compensated FI [5, 8, 12]. First, a measurement was taken of the radial distribution of the phase for a two-crystal FI (TGG in the [111] orientation) with quartz rotator but without polarizers. Then, based on the data obtained and constants of FK51 glass, we calculated the length of compensating glass that would be optimal for this FI, in this case 45 mm. The glass was placed between the FI and a lens 10 (Fig. 3). Between the lens and the CCD camera, a calcite wedge was used to separately observe vertical and horizontal polarization of the probe laser.

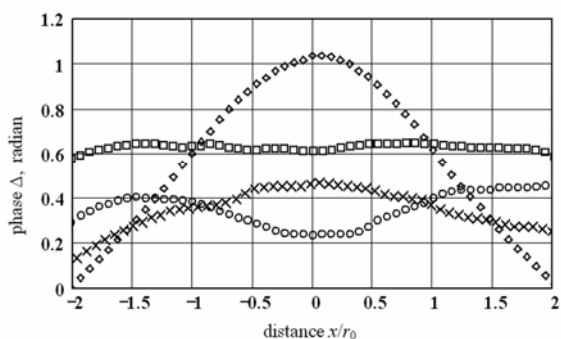


Fig. 7. Probe laser optical path difference after propagating through a birefringence-compensated FI without thermal compensation (diamonds) and with thermal compensation by means of FK51 glass:  $\phi$ -polarization (circles),  $r$ -polarization (crosses), average between two polarizations (squares). The heating laser power is 38 W.

The results of the measurements are presented in Fig. 7, which shows that the thermal lens averaged for two

polarizations (shown as squares) is almost totally compensated at a heating power of 38 W: at  $r < \sqrt{2} r_0$  (i.e., in the area of  $1/e^2$  by beam intensity) the difference of phase from constant is less than 0.02 radian. At the same time, the astigmatism of the resulting lens evident in the  $\phi$ -polarization (circles) and  $r$ -polarization (crosses) is very large, owing to the small ratio  $P_{FK51}/Q_{FK51}$ .

#### IV. DISCUSSION

The investigations that we have performed demonstrate that when calculating power losses of radiation in the spatial polarization mode, the photoelastic effect must be taken into account both in the magneto-optical medium and in the compensation glass. It is important to consider the isotropic change of the refractive index, characterized by the second component in expression (11) for  $P[001]$ , as well as anisotropic effects (characterized by parameter  $Q$ ), which lead to depolarization and amplitude-phase distortions.

First, we compare the relative contributions of the temperature dependence of refractive index and the photoelastic effect to the thermal lens (two components in expression (11) for  $P_{[001]}$ ). The value of  $(dn/dT)_{TGG}$  was measured in Ref. [28] and is  $19 \cdot 10^{-6} \text{ K}^{-1}$ , which coincides with the value  $20 \cdot 10^{-6} \text{ K}^{-1}$  reported in Refs. [19, 20]. Comparing this value with (35) we can conclude that the contribution of the photoelastic effect into the thermal lens is one third that of  $dn/dT$ , and signs of these effects are additive. For FK51 the value  $(dn/dT)_{FK51} = -7.3 \cdot 10^{-6} \text{ K}^{-1}$  is given in the catalogue for  $\lambda = 1064 \text{ nm}$  and weakly depends on the wavelength. The comparison of this value with (36) allows us to conclude (see the first eq. in (11)) that the contribution of the photoelastic effect in the parameter  $P$  is roughly 0.75 of the contribution of temperature dependence of the refractive index, and the signs of these effects are different, resulting in a value for  $P_{FK51}$  four times less than  $(dn/dT)_{FK51}$ .

Note that in reference [20] there is a statement that the contribution of the photoelastic effect in the thermal lens for TGG is 17% of that of  $dn/dT$ , and their signs are different. This is in fact incorrect, and arises from an incorrect interpretation of the photoelastic effect – formula (6) in reference [20] is incorrect. Referring to reference [20], the authors of reference [19] (which happen to be some of the same authors of this work), state that in many cases the contribution of the photoelastic effect is negligibly small in comparison with  $dn/dT$ , which, as follows from the above discussion, is incorrect either for TGG or for FK51.

A stronger thermal lens due to the photoelastic effect in TGG and a weaker thermal lens in FK51 can nevertheless have the same modulus and different signs provided the length of glass is chosen properly (considering the photoelastic effect) (see Fig. 6). However, the anisotropic part of the photoelastic effect in TGG leads to power losses in mode  $\gamma_p$  and  $\gamma_a$  that cannot be compensated. Moreover, the anisotropic part of the photoelastic effect induces additional losses. In this



regard, the figure-of-merit of glass is the ratio  $P_{CG}/Q_{CG}$ , which should be maximized for best performance. For the FK51 glass, this ratio is as small as 2.8, thereby considerably increasing  $\gamma_{aAC}$  and  $\gamma_{pAC}$ , (see formulas (18)). Figure 8 shows dependences of different losses plotted by formulas (17, 25, 27) taking into account the conditions (23, 24). Dashed lines indicate the dependences obtained by numerically integrating (2, 3) without the approximation of weak distortions used when deducing formulas (17, 25, 27). Although there is a small difference between the analytical and numerical results, it is evident that the analytical results fairly well describe  $\gamma$  in the limit  $\gamma < 0.1$ . As one can see from the Fig. 8, the telescope method is better than adaptive method with FK51 glass. This comes about because the figure of merit  $P_{FK51}/Q_{FK51} = 2.8$  is less than 3.2, the r.h.s of equ. (29b). However, telescopic compensation is a point design for a particular power; values plotted for telescopic compensation in Figure 8 assume that an optimal compensating focus is achieved at each power, requiring repositioning of the compensating lens. There are two ways of eliminating the negative influence of the anisotropic part of the photoelastic effect in the adaptive compensation method: by compensating the depolarization in the compensating element or by reducing its influence to a negligible level. The depolarization can be compensated using two elements made of FK51 glass and a 90° rotator of polarization placed between them, as it is performed in active elements of solid-state lasers [33]. If the total length of these two elements provides for condition (23), then the isotropic distortions in the FI will be compensated. This can be called ideal compensation, since, although the anisotropic part remains the same as without the compensating glass, yet:

$$\gamma_{IPC} = \gamma_{pNC} + \gamma_{aNC} \quad (39)$$

This method, however, has a disadvantage of complexity and losses associated with residual reflections from surfaces of additional elements.

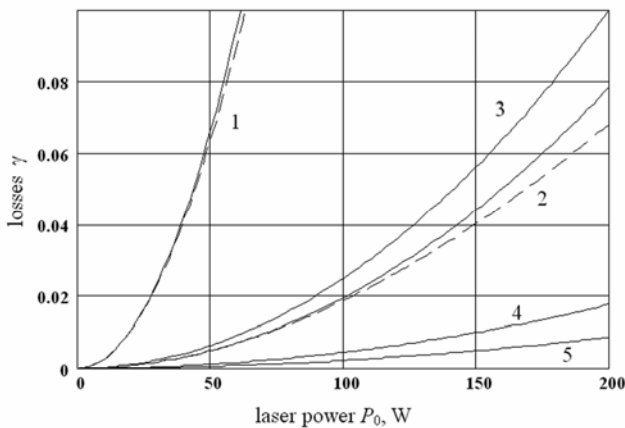


Fig. 8. Theoretically predicted power losses  $\gamma$  versus laser power  $P_0$  for the birefringence-compensated FI shown in Fig. 1b for no thermal compensation (curve 1), with telescope compensation (curve 2), adaptive compensation by means of FK51 (curve 3), by means of glass with  $P_{CG}/Q_{CG}=12$  (curve 4), by means of uniaxial crystal or gel (curve 5). The dashed lines show results of numerical integration and solid lines show analytical results given by formula (17, 25, 27, 39). For these calculations, we assumed a total length  $L=24\text{mm}$  of two TGG crystals, and TGG absorption  $\alpha_{TGG}=2.5 \cdot 10^{-3}\text{cm}^{-1}$ .

The effect of thermally induced anisotropy of the compensating glass can be considerably reduced by choosing a glass with a large ratio  $P_{CG}/Q_{CG}$ . It is seen from equ. 17, 18, 24-26, 31, and 35 that at  $P_{CG}/Q_{CG}=12$ , losses  $\gamma_{AC}$  during adaptive compensation are only twice as much as  $\gamma_{IPC}$  (see Fig. 8), and at  $P_{CG}/Q_{CG}>50$ , the negative influence of the compensating glass can be neglected in practice. Note, that compensating glass with  $Q_{CG}>0$  would be more preferable because in this case the last term in formula (18) for  $\gamma_{aAC}$  is negative ( $p<0$ ). The photoelastic effect can be totally eliminated by using gel as the compensating medium rather than glass, as it is done for compensation of the thermal lens in active laser media [34], or a crystal with natural birefringence, with which the induced birefringence can be neglected [23]. An example of such a crystal may be LICAF or YLF. The last one has [35]

$$\frac{dn}{dT} = \begin{cases} -2 \cdot 10^{-6} K^{-1} & \text{ordinary} \\ -4.3 \cdot 10^{-6} K^{-1} & \text{extraordinary} \end{cases}$$

To increase absorption, YLF can be doped by copper, ytterbium, or another element.

Note that in contrast to glass, a gel or an anisotropic crystal can be placed between polarizers of FI, without deteriorating the isolation ratio. This reduces the distance from the gel (or crystal) to TGG, thereby decreasing diffraction losses [19]. Another important advantage of YLF is that its thermal conductivity (6 W/Km [35]) and the product of thermal capacity (790 J/kgK) [35] and density (3.96 g/cm<sup>3</sup>) [35] are close to thermal conductivity and corresponding product of TGG crystal (thermal conductivity 385 J/kgK, density 7.32 g/cm<sup>3</sup>) [36]. Due to this, the thermal lens can be compensated not only in the stationary regime, but also dynamically in the presence of rapidly changing beam power. When gel or anisotropic crystal is used, the total power loss  $\gamma_i$  is described by (39). The dependence of  $\gamma_{IPC}$  on radiation power is plotted in Fig. 8. Here it is evident how efficient the adaptive compensation can be.

## V. CONCLUSION

We have performed a comprehensive investigation of thermally-induced self-action of laser beam propagation in TGG-based FIs. The absorption of laser power leads to losses in the initial spatial polarization mode of laser radiation. These losses  $\gamma_i$  consist of three components: losses induced by isotropic thermal lens  $\gamma_i$ ; polarization losses  $\gamma_p$ ; and losses associated with amplitude-phase distortions due to depolarization  $\gamma_a$ . The key parameters for determining  $\gamma_i$  are the thermo-optic constants  $P$ , which determines isotropic losses  $\gamma_i$ , and  $Q$ , which determines anisotropic losses  $\gamma_p + \gamma_a$ . We have measured these constants for TGG crystals and FK51 glass and find that for TGG, the contribution of the photoelastic effect to the isotropic component of the thermal lens is comparable in magnitude to the lens induced by  $dn/dT$ ,

and, because their contributions are additive, the actual thermal lens is stronger than the lens obtained when the photoelastic effect is neglected. For FK51 glass, the influence of the photoelastic effect is even higher. Thus, the contribution of the photoelastic effect in an isotropic thermal lens should be taken into account when the lens is compensated with an ordinary lens or a telescope with optimal focus [10] or using the adaptive method [19]. In the latter case, the figure-of-merit of the compensating glass is a ratio of thermo-optical constants  $P$  and  $Q$ . For the FK51 glass, the efficiency of the adaptive method is less than for the ordinary lens with an optimal focus, because the value of  $P/Q$  for this glass is small. However, the efficiency of the adaptive compensation can be considerably enhanced by eliminating the anisotropy with a  $90^\circ$  polarization rotator or using a compensating glass with  $P_{CG}/Q_{CG} > 50$ , such as a crystal with natural birefringence or a gel.

## VI. ACKNOWLEDGMENT

The authors gratefully acknowledge the support of the National Science Foundation (grants PHY0140110 and PHY0244902) in support of this research.

## REFERENCES

- [1] V. Gapontsev and W. Krupke, "Fiber lasers grow in power," *Laser focus World*, vol. 38, pp. 83-87, 2002.
- [2] Y. Akiyama, H. Takada, H. Yuasa, and N. Nishida, "Efficient 10 kW diode-pumped Nd:YAG rod laser," presented at Advance Solid State Lasers, Quebec City, Canada, 2002.
- [3] A. N. Malshakov, G. Pasmanik, and A. K. Potemkin, "Comparative characteristics of magneto-optical materials," *Applied Optics*, vol. 36, pp. 6403-6410, 1997.
- [4] T. V. Zarubina, A. N. Mal'shakov, G. A. Pasmanik, and A. K. Potemkin, "Comparative characteristics of magneto-optical glasses," *Opticheskiy zhurnal*, vol. 64, pp. 67-71, 1997.
- [5] E. A. Khazanov, "Compensation of Thermally Induced Polarization Distortions in Faraday Isolators," *Quantum Electronics*, vol. 29, pp. 59-64, 1999.
- [6] E. A. Khazanov, O. V. Kulagin, S. Yoshida, D. Tanner, and D. Reitze, "Investigation of Self-Induced Depolarization of Laser Radiation in Terbium Gallium Garnet," *IEEE J. of Quantum Electronics*, vol. 35, pp. 1116-1122, 1999.
- [7] H. J. Eichler, O. Mehl, and J. Eichler, "Multi-amplifier arrangements with phase conjugation for power scaling of solid state lasers with high beam quality," presented at Proc. SPIE, 1999.
- [8] E. Khazanov, N. Andreev, A. Babin, A. Kiselev, O. Palashov, and D. Reitze, "Suppression of Self-Induced Depolarization of High-Power Laser Radiation in Glass-Based Faraday Isolators," *JOSA B*, vol. 17, pp. 99-102, 2000.
- [9] N. Andreev, A. Babin, A. Kiselev, O. Palashov, E. Khazanov, O. Shavelov, and T. Zarubina, "Thermo-optical constant of magneto-active glasses," *Journal of optical technology*, vol. 67, pp. 556-558, 2000.
- [10] E. A. Khazanov, "Characteristic features of the operation of different designs of the Faraday Isolator for high average laser-radiation power," *Quantum Electronics*, vol. 30, pp. 147-151, 2000.
- [11] E. A. Khazanov, "High-power propagation effects in different designs of a Faraday isolator," presented at Optical Pulse and Beam Propagation II, 2000.
- [12] N. F. Andreev, O. V. Palashov, A. K. Poteomkin, A. M. Sergeev, E. A. Khazanov, and D. H. Reitze, "45dB Faraday isolator for 100W average radiation power," *Quantum Electronics*, vol. 30, pp. 1107-1108, 2000.
- [13] K. S. Lai, R. Wu, and P. B. Phua, "Multiwatt KTiOPO<sub>4</sub> Optical Parametric Oscillators Pumped within Randomly and Linearly Polarized Nd:YAG Laser Cavities," presented at Nonlinear Materials, Devices and Applications, 2000.
- [14] E. Khazanov, N. Andreev, O. Palashov, A. Poteomkin, A. Sergeev, O. Mehl, and D. Reitze, "Effect of terbium gallium garnet crystal orientation on the isolation ratio of a Faraday isolator at high average power," *Applied Optics*, vol. 41, pp. 483-492, 2002.
- [15] N. F. Andreev, E. V. Katin, O. V. Palashov, A. K. Potemkin, D. Reitze, A. M. Sergeev, and E. A. Khazanov, "The use of crystalline quartz for compensation for thermally induced depolarization in Faraday isolators," *Quantum Electronics*, vol. 32, pp. 91-94, 2002.
- [16] M. R. Ostermeyer, G. Klemz, P. Kubina, and R. Menzel, "Quasi-continuous-wave birefringence-compensated single- and double-rod Nd:YAG lasers," *Applied Optics*, vol. 41, pp. 7573-7582, 2002.
- [17] K. A. Strain, K. Danzmann, J. Muzino, P. G. Nelson, A. Rudiger, R. S. Schilling, and W. Winkler, "Thermal Lensing in Recycling Interferometric Gravitational-Wave Detectors," *Physics Letters A*, vol. 194, pp. 124-132, 1994.
- [18] C. A. Denman and S. I. Libby, "Birefringence Compensation using a Single Nd:YAG Rod," *OSA TOPS*, vol. 26, pp. 608-612, 1999.
- [19] G. Mueller, R. S. Amin, D. Guagliardo, D. McFeron, R. Lundock, D. H. Reitze, and D. B. Tanner, "Method for compensation of thermally induced modal distortions in the input optical components of gravitational wave interferometers," *Classical and Quantum Gravity*, vol. 19, pp. 1793-1801, 2002.
- [20] J. D. Mansell, J. Hennawi, E. K. Gustafson, M. M. Fejer, R. L. Byer, D. Clubley, S. Yoshida, and D. H. Reitze, "Evaluating the effect of transmissive optic thermal lensing on laser beam quality with a Shack - Hartmann wave-front sensor," *Applied Optics*, vol. 40, pp. 366-374, 2001.
- [21] A. P. Voytovich and V. N. Severikov, *Lasers with anisotropic resonators*. Minsk: Nauka i tehnika, 1988.
- [22] M. J. Tabor and F. S. Chen, "Electromagnetic Propagation through Materials Possessing Both Faraday Rotation and Birefringence: Experiments with Ytterbium Orthoferrite," *Applied Physics*, vol. 40, pp. 2760-2765, 1969.
- [23] A. V. Mezenov, L. N. Soms, and A. I. Stepanov, *Thermo-optics of solid-state lasers*. Leningrad: Mashinostroenie, 1986.
- [24] W. Koechner, "Thermal Lensing in a Nd: YAG Laser Rod," *Applied Optics*, vol. 9, pp. 2548-2553, 1970.
- [25] A. Anan'ev, N. A. Kozlov, A. A. Mak, and A. I. Stepanov, "Thermal distortion of solid state laser cavity," *Prikladnaya spektroskopiya*, vol. 5, pp. 51-55, 1966.
- [26] L. N. Soms and A. A. Tarasov, "Thermal Deformation in Color-Center Laser Active Elements. 1.Theory," *Soviet Journal of Quantum Electronics*, vol. 9, pp. 1506-1508, 1979.
- [27] A. A. Mak, L. N. Soms, V. A. Fromzel, and V. E. Yashin, *Nd:glass lasers*. Moscow: Nauka, 1990.
- [28] A. Poteomkin, N. Andreev, E. Khazanov, A. Shaykin, V. Zelenogorsky, and I. Ivanov, "Use of scanning Hartmann sensor for measurement of thermal lensing in TGG crystal," presented at Laser Crystals, Glasses, and Nonlinear Materials Growth and Characterization III, 2003.
- [29] A. Anan'ev and N. I. Grishmanova, "Deformation of active elements of interferometer and thermo-optical constant Nd: glass," *Prikladnaya spektroskopiya*, vol. 12, pp. 668-673, 1970.
- [30] A. A. Mak, V. M. Mit'kin, and L. N. Soms, "About thermo-optical constant of doped glasses," *Optiko-mekhanicheskay promishlennost*, vol. 9, pp. 65-66, 1971.
- [31] M. Born and E. Wolf, *Principles of Optics*. New York: Pergamon, 1980.
- [32] M. Abitbol, X. Ben-Yosef, and N. Nissim, "Use of the Hartmann sensor to measure the unisoplanatic wavefront tilt," *Applied Optics*, vol. 30, pp. 1512-1523, 1991.
- [33] W. C. Scott and M. de Wit, "Birefringence Compensation and TEM<sub>00</sub> Mode Enhancement in a Nd:YAG Laser," *Applied Physics Letters*, vol. 18, pp. 3-4, 1971.
- [34] T. Graf, E. Wyss, M. Roth, and H. P. Weber, "Adaptive thermal optics in high-power laser resonators," presented at Proc. SPIE, Laser Resonators and Beam Control, 2002.
- [35] G. M. Zverev and D. Golyaev, *Crystalline lasers and its application*. Moscow: Radio and sviaz, 1994.
- [36] T. V. Zarubina, Private communication.